All-Optical Control of Linear and Nonlinear Energy Transfer via the Zeno Effect

Xiang Guo,[1] Chang-Ling Zou,[1,2,3] Liang Jiang,[2] and Hong X. Tang[1,*]
[1]Department of Electrical Engineering, Yale University, New Haven, Connecticut 06511, USA
[2]Department of Applied Physics, Yale University, New Haven, Connecticut 06511, USA
[3]Key Laboratory of Quantum Information, University of Science and Technology of China, Hefei, Anhui 230026, China

(Received 21 January 2018; published 16 May 2018)

Microresonator-based nonlinear processes are fundamental to applications including microcomb generation, parametric frequency conversion, and harmonics generation. While nonlinear processes involving either second- ($\chi^{(2)}$) or third- ($\chi^{(3)}$) order nonlinearity have been extensively studied, the interaction between these two basic nonlinear processes has seldom been reported. In this paper we demonstrate a coherent interplay between second- and third- order nonlinear processes. The parametric ($\chi^{(2)}$) coupling to a lossy ancillary mode shortens the lifetime of the target photonic mode and suppresses its density of states, preventing the photon emissions into the target photonic mode via the Zeno effect. Such an effect is then used to control the stimulated four-wave mixing process and realize a suppression ratio of 34.5.

DOI: 10.1103/PhysRevLett.120.203902

Introduction.—The ancient Zeno's arrow paradox describes that a flying arrow seems to be not moving if it is instantly observed. Such a concept is generalized to the quantum Zeno effect (QZE) by Sudarshan *et al.* [1], which states that the evolution of a quantum system can be frozen by the frequent measurement. In theory, the measurement of a system will have an effect on the dynamics of that system, shifting the effective energy level of a quantum system or changing its decay rate. Zeno effects inherently result from such measurement backaction. Apart from the frequent measurement, the Zeno effect can be equivalently realized by a continuous strong coupling to an ancillary system, which has been proved theoretically and experimentally [2–4]. Such effects have been widely applied in quantum system control and engineering, including quantum state preparation [5–11], entanglement generation [10], autonomous quantum error correction [12,13], and even counterfactual quantum communication [14].

In recent years, cavity nonlinear optical processes have been widely explored due to their important applications on Kerr comb generation [15–20], frequency conversion [21–24], new wavelength generation [25–28], and correlated photon pair generation [29–31]. As an analogue of a quantum system, a photonic mode in the microcavity can be treated as an energy level that allows multiple excitation. Therefore, we could expect similar engineering and control of the photonic mode by the Zeno effect [32,33]. It is proposed and demonstrated that the optical switching based on the Zeno effect can be realized by cavity nonlinear optical effects [34–38]. However, only one optical nonlinear process is involved in previous experiments and only the linear energy transfer in the system is controlled by the Zeno effect.

In this Letter, we demonstrate a coherent interaction between the second- ($\chi^{(2)}$) and third- ($\chi^{(3)}$) order nonlinear process in an aluminum nitride (AlN) microring resonator. We show that not only the linear coupling, but also the nonlinear frequency conversion process, can be greatly suppressed by the Zeno effect. Specifically, we utilize the strong second-order optical nonlinearity in an AlN microring resonator to coherently couple the target high-Q photonic mode to a low-Q ancillary mode. The coherent coupling to a lossy ancillary mode shortens the lifetime of the target photonic mode and suppresses its density of states, preventing the photon emissions into the target photonic mode via the Zeno effect. We first verify the Zeno effect by probing the suppressed linear energy transfer between the external waveguide and the microcavity. Such a Zeno effect is then used to control the nonlinear frequency conversion process inside the cavity, where the photon generated in the target mode through the stimulated four-wave mixing (FWM) process is suppressed by a factor of 34.5.

System and model.—As a material possessing both $\chi^{(2)}$ and $\chi^{(3)}$ nonlinearity [39], AlN has been used to realize high-efficiency second-harmonic generation [28] (using $\chi^{(2)}$) and third-harmonic generation [40] (using $\chi^{(3)}$). It is worth noting that the simultaneous generation of both second and third harmonics has also been observed in the case of extreme nonlinear optics [41], where both nonlinear optical processes originate from $\chi^{(3)}$ nonlinearity. Our experimental system contains a waveguide coupled AlN microring resonator [23,28], which supports a variety of optical modes of different wavelengths. In the following study, we focus on three optical modes located in the telecom band (a, b, c) and one optical mode in the visible band (d). When the microring is cold, i.e., not pumped by any laser, the density of states of all these optical modes are shown in Fig. 1(a). The telecom optical modes (a, b, c) have a higher and narrower density of states because of

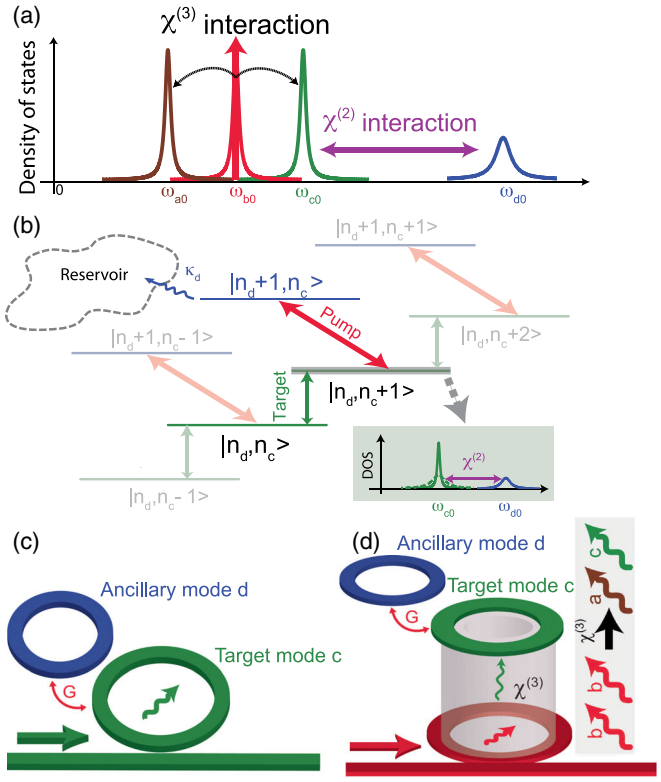

FIG. 1. Schematic and the energy diagram of optical modes coupling through $\chi^{(2)}$ and $\chi^{(3)}$ nonlinearity. (a) The linear density of states of the system. Optical modes a, b, and c are coupled through the $\chi^{(3)}$ process while b, c, and d are coupled through the $\chi^{(2)}$ process. (b) The energy diagram describing the nonlinear coupling between the target photonic mode c and the ancillary photonic mode d via the three-wave mixing process. $n_c(n_d)$ stands for the cavity photon number for mode c (d). Inset: the dramatically suppressed density of states for the target mode when coherently coupled to the ancillary mode. (c) Probing the Zeno effect with a linear waveguide-to-microring coupling scheme. (d) Controlling the nonlinear wavelength conversion process the via the Zeno effect. The photon emissions into the targeted optical mode via the four-wave mixing process are suppressed when the target optical mode is coupled to the dissipative ancillary mode.

their longer lifetime (~210 ps) compared to the visible mode d (~45 ps). The third-order nonlinear interaction leads to a FWM process where two photons in mode b are converted to a pair of photons in mode a and c ($b+b\rightarrow a+c$), as illustrated in Fig. 1(a). Because of the second-order nonlinear effect, modes b, c are also participating in the three-wave mixing (TWM) process ($b+c\rightarrow d$) which involves the high-loss visible mode d. Under a pump at mode b, the system can be described by the Hamiltonian [42]

$$\frac{H}{\hbar}=\sum_{o\in\{a,b,c,d\}}\omega_{o,0}\hat{o}^{\dagger}\hat{o}+g_2(\hat{b}^{\dagger}\hat{c}^{\dagger}\hat{d}+\text{c.c.}) +g_3[(\hat{b}^{\dagger})^2\hat{a}\,\hat{c}+\text{c.c.}]+\epsilon_b(i\hat{b}^{\dagger}e^{-i\omega_b t}+\text{c.c.}). \quad (1)$$

Here, $\hat{o}$ is the Bosonic operator for mode o with $o\in\{a,b,c,d\}$, and $\omega_{o,0}$ is the angular frequency of mode o. The intrinsic, external, and total loss rate of mode o are denoted as $\kappa_{o,0}$, $\kappa_{o,1}$ and $\kappa_o=\kappa_{o,0}+\kappa_{o,1}$, respectively. The input pump field $\epsilon_b=\sqrt{2\kappa_{b,1}P_b/\hbar\omega_b}$, where P_b and ω_b are the power and frequency of the pump laser, respectively. g_2 and g_3 are the single-photon nonlinear coupling strength for the TWM and FWM processes, respectively. The numerical values for all the relevant parameters are summarized in the Supplemental Material [42].

Under a strong coherent pump field in mode b, the photons in mode c can be coherently converted to the high-loss mode d and get dissipated to the environment [Fig. 1(b)]. For the sake of convenience, in the following context we name the long-lifetime mode c as the "target" photonic mode and the short-lifetime mode d as the "ancillary" mode. This coherent coupling between the target mode c and the ancillary mode d can be regarded as a continuous measurement of mode c. And the backaction of such measurement leads to a counterfactual result that the ability for the photons to couple into the target mode c is suppressed. This is an analogue to the Zeno effect where frequent measurement inhibits the occupation of an energy level. Alternatively, we can understand the Zeno effect as the reduction of the density of states, as shown in the inset of Fig. 1(b), due to coupling with the dissipative ancillary mode.

Linear probe of the Zeno effect.—To experimentally verify the Zeno effect induced by the TWM, we directly probe the linear energy transfer from the external waveguide to the target mode c, which has been employed in previous related works [34–38]. This linear probe scheme is shown in Fig. 1(c), where a bus waveguide is used to send photons into the target photonic mode through the evanescent coupling between the waveguide and the microring.

When the dissipative ancillary mode is parametrically coupled with the target mode via the TWM process, the photons remain in the bus waveguide with suppressed coupling into the microring. Quantitatively, when scanning the frequency of the probe laser (ω_c) across the resonance of the target mode c, the transmission spectrum can be calculated as [42]

$$t_c=\left|1+\frac{2\kappa_{c,1}}{-i\delta_c-\kappa_c+\frac{g_2^2|\beta|^2}{(-i\delta_d-\kappa_d)}}\right|^2. \quad (2)$$

Here, $\delta_c=\omega_{c0}-\omega_c$ and $\delta_d=\omega_{d0}-\omega_b-\omega_c$ are the frequency detunings for mode c and d, respectively, which are expressed in terms of the pump frequency ω_b and probe frequency ω_c. $\beta=\epsilon_b/[-i(\omega_{b,0}-\omega_b)-\kappa_b]$ represents the pump mode field under the nondepletion approximation. Compared with the transmission spectrum of c without the pump ($\beta=0$) that $t_c=|1+2\kappa_{c,1}/(-i\delta_c-\kappa_c)|^2$, a maximum modification of the target mode's transmission will happen when the phase-matching condition for the TWM process is fulfilled, i.e., $\delta_{\text{pm}}\triangleq\omega_{d0}-(\omega_b+\omega_{c0})=0$, which physically mean that mode c (with a resonant frequency

ω_{c0}) and d (with a resonant frequency ω_{d0}) are resonant coupled to each other in the rotating frame of the pump laser frequency ω_b. When phase matched, the coherent coupling to the ancillary mode d introduces an extra loss term $\gamma = g_2^2|\beta|^2/\kappa_d$ to κ_c. When the coupling to the ancillary mode is very strong, i.e., $\gamma \gg \kappa_c$, the coherent coupling will quickly dissipate any photons that couple into the target photonic mode c. This leads to a counterfactual result that the ability for the photons to couple into the target mode c is suppressed and results in a much larger transmission t_c, as we will show next.

The experimental setup is illustrated in Fig. 2(a). One pump laser is used to coherently drive the optical mode b, acting as the pump for the TWM process. The on-chip power of the pump laser varies from 0 to around 180 mW. In experiment, we scan the frequency of pump laser ω_b across the resonance of the pump mode b. Since the value of $\delta_{\rm pm}$ is very important for observing the Zeno effect, we first explain the tuning of $\delta_{\rm pm}$ during the pump laser scan. Because of the thermal effects, a frequency redshift will happen when scanning the pump laser, which results in an extended transmission spectrum with a triangle shape [43]. Figure 2(b) shows a typical pump laser transmission spectrum. The thermal effects induced by the pump would also affect the other resonances in the same microring cavity, albeit at different rate. As a result, the value of $\delta_{\rm pm}$ will also change during the pump laser scanning process [Fig. 2(c)]. It is indicated that at a certain pump wavelength, the phase-matching condition $\delta_{\rm pm} = 0$ is satisfied. In this condition, the target mode c will be *resonantly* coupled to the ancillary mode d and the effect of TWM will be prominent.

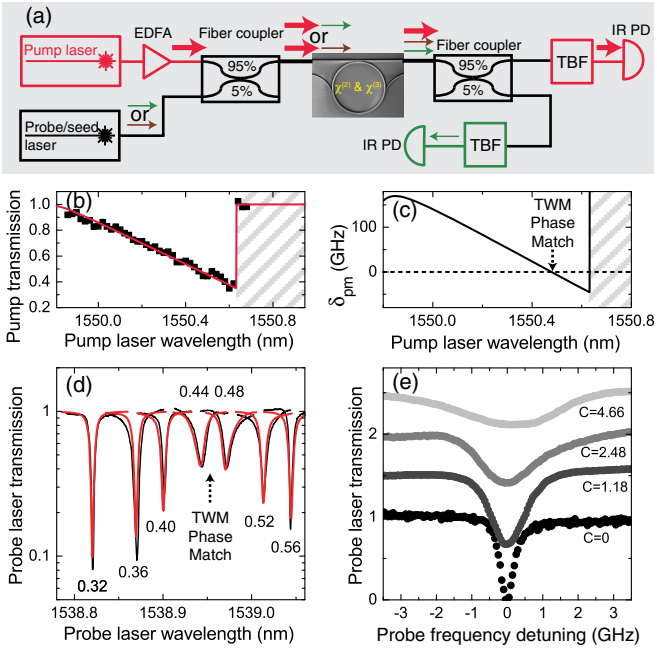

FIG. 2. Probing the Zeno effect with the linear coupling scheme. (a) Experimental setup. A strong laser is used to coherently drive the optical mode b. A probe laser can either directly probe the Zeno effect using the linear coupling scheme by scanning across the resonance of the target photonic mode c or using the nonlinear scheme by scanning across the resonance of mode a. Tunable bandpass filter (TBF). (b) The transmitted power of the strong pump laser when scanning across the resonance of mode b. A trianglelike shape is observed due to the thermal effect. (c) The tuning of phase mismatch $\delta_{\rm pm}$ during the pump laser wavelength scan. At a certain pump wavelength the phase-match condition is fulfilled. (d) The measured transmission spectra of the target photonic mode c under different pump laser wavelength. The pump laser wavelength ($\lambda_b - 1550$ nm) is labeled near each curve. When the phase mismatch gradually approaches 0, a much lower-extinction resonance dip is observed. The black curves are experimental data, which agree with the red theoretical curves. (e) The measured transmission of the target photonic mode c with phase-matching condition $\delta_{\rm pm} = 0$ satisfied. With larger pump laser photon number (hence larger cooperativity C), the mode c's extinction is reduced and the Zeno effect is more prominent.

In the experiment, we measure the transmission spectrum of the target mode c during each scanning step of pump laser ω_b. Each step corresponds to a different phase mismatch $\delta_{\rm pm}$ and pump laser field β. The on-chip probe laser power was set to be 0.1 mW, much weaker than the pump laser power. In the measured transmission spectra of the target mode c [Fig. 2(d)], we can see that originally the transmission is of normal Lorentzian shape, which corresponds to the situation where the TWM is not prominent due to an unsatisfied phase-matching condition ($\delta_{\rm pm} \gg \kappa_c$). The photons from bus waveguide can be efficiently coupled to the target photonic mode, leading to a high-extinction dip in the transmission spectrum. At a certain point, when the phase mismatch $\delta_{\rm pm} = 0$ and β is considerably large, a broadened transmission spectrum of the target mode c is observed. Noticeably, the much shallower extinction dip manifests itself as an indication of Zeno effect, with suppressed coupling between the bus waveguide and the microring. As the pump laser wavelength changes further, the coupling to the ancillary mode gets lost due to an unsatisfied phase-matching condition ($\delta_{\rm pm} \neq 0$) and the spectrum of the target mode c returns to the high-extinction Lorentzian shape. We observe in Fig. 2(d) that the simulated transmission spectra (red) of mode c matches very well with the measured curve (black), indicating a good theoretical understanding of this process. By increasing the power of the pump laser, the cooperativity [23] $C = (g_2^2|\beta|^2/\kappa_c\kappa_d)$ of the TWM process will increase proportionally. We can therefore observe the suppression of the linear coupling with increasing fidelity, as shown in Fig. 2(e).

Controlling FWM via the Zeno effect.—As the Zeno effect by TWM is confirmed by measuring the linear energy transfer in the system, we then investigate how the Zeno effect can be used to control the nonlinear processes in the cavity. Specifically, we study the

suppression of photon generation in the target mode through the stimulated FWM, which is a nonlinear energy transfer process, as depicted in Fig. 1(d). By controlling the temperature of the photonic chip, we can determine whether the phase-matching condition of the TWM process can be fulfilled [28]. As we show next, by switching on and off the TWM process, we can control the FWM efficiency by more than 1 order of magnitude.

At certain temperature, the phase-matching condition is not fulfilled, i.e., $g_2^2|\beta|^2/\delta_d \ll \kappa_c$, and TWM's effect is negligible. In this case, we can study the pure FWM process, i.e., ignoring the $\chi^{(2)}$ related term in the system's Hamiltonian. As mode b is strongly pumped by a pump laser with frequency ω_b, we stimulate the FWM process by sending a seed laser around mode a and record the generated light intensity in the target mode c. The nonlinear energy transfer to the target mode c through the FWM process can be calculated by [42]

$$P_{\mathrm{c,out}} = \frac{2\kappa_{a,1}}{\delta_a^2+\kappa_a^2}\frac{2\kappa_{c,1}}{\delta_c^2+\kappa_c^2}\frac{\omega_c}{\omega_a}|\beta^4|g_3^2 P_{\mathrm{a,in}}, \tag{3}$$

where $P_{\mathrm{a,in}}$ is the input power of the seed laser around mode a. During the scanning of pump laser ω_b, the pump laser frequency gradually approaches the resonance of mode b and suddenly jumps out of resonance due to thermal bistability, which is already explained and shown in Fig. 2(b). By considering the thermal induced frequency shift into Eq. (3), the normalized efficiency of the stimulated FWM as a function of both pump laser wavelength and seed laser wavelength can be estimated, as shown in Fig. 3(a). By extracting the maximum stimulated FWM efficiency at each pump wavelength [Fig. 3(c)], we observe that the photon emissions in the target mode c through stimulated FWM increases monotonically with the pump wavelength approaching the resonance of mode b.

By tuning the device's temperature, we can fulfill the phase-matching condition for the TWM process. We then consider the case when the TWM exists and couples the target mode c with an ancillary mode d. In this case, the nonlinear energy transfer to the target mode is modified as

$$P'_{\mathrm{c,out}} = P_{\mathrm{c,out}}\Big/\left|1+\frac{g_2^2|\beta|^2}{(-i\delta_d-\kappa_d)(-i\delta_c-\kappa_c)}\right|^2. \tag{4}$$

The additional term $([g_2^2|\beta|^2]/[(-i\delta_d-\kappa_d)(-i\delta_c-\kappa_c)])$ due to coherent coupling between mode c and d can lead to a dramatic decrease of the nonlinear energy transfer efficiency. The numerical simulation of the stimulated FWM process when the TWM is involved is shown in Fig. 3(b). Compared to Fig. 3(a), a clear suppression of the efficiency is observed when the phase-matching condition ($\delta_{\mathrm{pm}} = 0$) of TWM process is satisfied. Again we extract the maximum stimulated FWM efficiency at each pump wavelength, as shown in Fig. 3(d). A clear dip of FWM

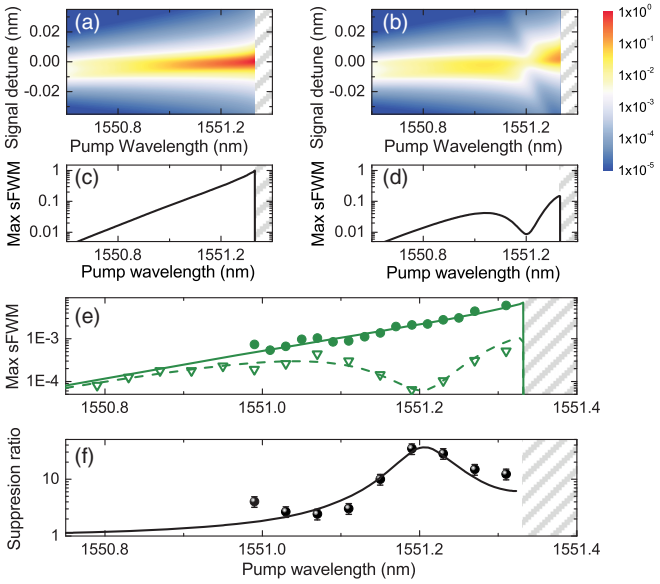

FIG. 3. Numerical simulation and experimental measurement of the suppressed four-wave mixing efficiency due to the Zeno effect. (a)–(b) The intensity of stimulated four-wave mixing in target mode c (a) with or (b) without the $\chi^{(2)}$ process. The signal laser is scanning across mode a while the pump laser is scanning across mode b. (c)–(d) The maximum stimulated four-wave mixing intensity as the pump laser scanning across mode b when the $\chi^{(2)}$ interaction (c) does not show up (d) shows up. (e) Experimental result of the stimulated four-wave mixing efficiency with and without $\chi^{(2)}$ interaction. The solid circles (without $\chi^{(2)}$) and open triangles (with $\chi^{(2)}$) represent the experimental measurements while the solid (without $\chi^{(2)}$) and dashed (with $\chi^{(2)}$) lines corresponds to theoretical fitting. (f) The suppression ratio of four-wave mixing efficiency as a function of the pump wavelength.

efficiency appears when the phase-matching condition is satisfied. This suppressed FWM efficiency signifies the appearance of the Zeno effect in the nonlinear energy transfer process.

The experimental results about such suppression of stimulated FWM are summarized in Figs. 3(e) and 3(f). When the TWM is negligible, the measured stimulated FWM efficiency depends on the pump wavelength as shown by the solid circles in Fig. 3(e). In contrast, when the phase-matching condition of TWM process is fulfilled, a clear suppression of FWM efficiency is shown by the open triangles as depicted in Fig. 3(e). The solid and dashed lines come from the theoretical fitting and the used fitting parameters are summarized in the Supplemental Material [42]. To quantify the suppression of nonlinear frequency conversion process induced by the Zeno effect, we plot the suppression ratio against the pump wavelength, as shown in Fig. 3(f). It can be observed that at a certain pump wavelength, when the phase matching of TWM is satisfied, the highest suppression ratio of 34.5 is achieved. This large suppression ratio clearly demonstrates the control of the system's nonlinear dynamics utilizing the Zeno effect. Note

that the experimental result deviates slightly from the theoretical curve at the pump wavelength close to 1551.0 nm. This could be induced by the weak backscattering inside the microring, which is not considered in the theoretical model.

Conclusion.—We have investigated the all-optical control of linear and nonlinear energy transfer in a nonlinear microring cavity by combining the TWM and FWM processes. We show that the efficiency of stimulated FWM is suppressed by a factor of 34.5 through Zeno control, which is implemented by coherently coupling the target photonic mode to the high-loss ancillary mode. The demonstrated Zeno control on a photonic chip can be a useful tool for tailoring the local mode's density of state and the dispersion, suppressing or enhancing the nonlinear optics process. The ample nonlinear effects in the microcavity may also lead to potential applications in quantum nonlinear optics, such as entangled photon pairs generation [44,45] and *in situ* frequency conversion [23,24,46] into other wavelength bands.

Facilities used for device fabrication were supported by the Yale SEAS cleanroom and the Yale Institute for Nanoscience and Quantum Engineering. The authors thank Michael Power and Dr. Michael Rooks for assistance in device fabrication. We acknowledge funding support from an AFOSR MURI Grants (No. FA9550-15-1-0029, No. FA9550-15-1-0015), LPS/ARO Grant (No. W911NF-14-1-0563), NSF EFRI Grant (No. EFMA-1640959), the DARPA SCOUT program, and the Packard Foundation. L. J. acknowledges support from the Alfred P. Sloan Foundation (BR2013-049) and the Packard Foundation (2013-39273).

*hong.tang@yale.edu

[1] B. Misra and E. C. G. Sudarshan, The Zeno's paradox in quantum theory, J. Math. Phys. **18**, 756 (1977).
[2] A. G. Kofman and G. Kurizki, Universal Dynamical Control of Quantum Mechanical Decay: Modulation of the Coupling to the Continuum, Phys. Rev. Lett. **87**, 270405 (2001).
[3] P. Facchi, D. A. Lidar, and S. Pascazio, Unification of dynamical decoupling and the quantum Zeno effect, Phys. Rev. A **69**, 032314 (2004).
[4] F. Schäfer, I. Herrera, S. Cherukattil, C. Lovecchio, F. Cataliotti, F. Caruso, and A. Smerzi, Experimental realization of quantum zeno dynamics, Nat. Commun. **5**, 3194 (2014).
[5] G. J. Milburn, Quantum Zeno effect and motional narrowing in a two-level system, J. Opt. Soc. Am. B **5**, 1317 (1988).
[6] W. M. Itano, D. J. Heinzen, J. J. Bollinger, and D. J. Wineland, Quantum Zeno effect, Phys. Rev. A **41**, 2295 (1990).
[7] A. G. Kofman and G. Kurizki, Quantum Zeno effect on atomic excitation decay in resonators, Phys. Rev. A **54**, R3750 (1996).
[8] J. M. Raimond, C. Sayrin, S. Gleyzes, I. Dotsenko, M. Brune, S. Haroche, P. Facchi, and S. Pascazio, Phase Space Tweezers for Tailoring Cavity Fields by Quantum Zeno Dynamics, Phys. Rev. Lett. **105**, 213601 (2010).
[9] A. Signoles, A. Facon, D. Grosso, I. Dotsenko, S. Haroche, J.-M. Raimond, M. Brune, and S. Gleyzes, Confined quantum Zeno dynamics of a watched atomic arrow, Nat. Phys. **10**, 715 (2014).
[10] G. Barontini, L. Hohmann, F. Haas, J. Esteve, and J. Reichel, Deterministic generation of multiparticle entanglement by quantum Zeno dynamics, Science **349**, 1317 (2015).
[11] L. Bretheau, P. Campagne-Ibarcq, E. Flurin, F. Mallet, and B. Huard, Quantum dynamics of an electromagnetic mode that cannot contain N photons, Science **348**, 776 (2015).
[12] N. Erez, Y. Aharonov, B. Reznik, and L. Vaidman, Correcting quantum errors with the Zeno effect, Phys. Rev. A **69**, 062315 (2004).
[13] G. A. Paz-Silva, A. T. Rezakhani, J. M. Dominy, and D. A. Lidar, Zeno Effect for Quantum Computation and Control, Phys. Rev. Lett. **108**, 080501 (2012).
[14] Y. Cao, Y.-H. Li, Z. Cao, J. Yin, Y.-A. Chen, H.-L. Yin, T.-Y. Chen, X. Ma, C.-Z. Peng, and J.-W. Pan, Direct counterfactual communication via quantum Zeno effect, Proc. Natl. Acad. Sci. U.S.A. **114**, 4920 (2017).
[15] P. Del'Haye, A. Schliesser, O. Arcizet, T. Wilken, R. Holzwarth, and T. J. Kippenberg, Optical frequency comb generation from a monolithic microresonator, Nature (London) **450**, 1214 (2007).
[16] T. Herr, V. Brasch, J. D. Jost, C. Y. Wang, N. M. Kondratiev, M. L. Gorodetsky, and T. J. Kippenberg, Temporal solitons in optical microresonators, Nat. Photonics **8**, 145 (2014).
[17] X. Xue, Y. Xuan, Y. Liu, P.-H. Wang, S. Chen, J. Wang, D. E. Leaird, M. Qi, and A. M. Weiner, Mode-locked dark pulse Kerr combs in normal-dispersion microresonators, Nat. Photonics **9**, 594 (2015).
[18] Q.-F. Yang, X. Yi, K. Y. Yang, and K. Vahala, Stokes solitons in optical microcavities, Nat. Phys. **13**, 53 (2017).
[19] M. Yu, Y. Okawachi, A. G. Griffith, M. Lipson, and A. L. Gaeta, Mode-locked mid-infrared frequency combs in a silicon microresonator, Optica **3**, 854 (2016).
[20] X. Guo, C.-L. Zou, H. Jung, Z. Gong, A. Bruch, L. Jiang, and H. X. Tang, Efficient visible frequency comb generation via Cherenkov radiation from a Kerr microcomb, arXiv:1704.04264.
[21] J. Huang and P. Kumar, Observation of quantum frequency conversion, Phys. Rev. Lett. **68**, 2153 (1992).
[22] K. De Greve, L. Yu, P. L. McMahon, J. S. Pelc, C. M. Natarajan, N. Y. Kim, E. Abe, S. Maier, C. Schneider, M. Kamp, S. Höfling, R. H. Hadfield, A. Forchel, M. M. Fejer, and Y. Yamamoto, Quantum-dot spin-photon entanglement via frequency downconversion to telecom wavelength, Nature (London) **491**, 421 (2012).
[23] X. Guo, C.-L. Zou, H. Jung, and H. X. Tang, On-Chip Strong Coupling and Efficient Frequency Conversion between Telecom and Visible Optical Modes, Phys. Rev. Lett. **117**, 123902 (2016).
[24] Q. Li, M. Davanço, and K. Srinivasan, Efficient and low-noise single-photon-level frequency conversion interfaces using silicon nanophotonics, Nat. Photonics **10**, 406 (2016).

[25] S. M. Spillane, T. J. Kippenberg, and K. J. Vahala, Ultralow-threshold Raman laser using a spherical dielectric microcavity, Nature (London) **415**, 621 (2002).

[26] T. Carmon and K. J. Vahala, Visible continuous emission from a silica microphotonic device by third-harmonic generation, Nat. Phys. **3**, 430 (2007).

[27] J. U. Fürst, D. V. Strekalov, D. Elser, M. Lassen, U. L. Andersen, C. Marquardt, and G. Leuchs, Naturally Phase-Matched Second-Harmonic Generation in a Whispering-Gallery-Mode Resonator, Phys. Rev. Lett. **104**, 153901 (2010).

[28] X. Guo, C.-L. Zou, and H. X. Tang, Second-harmonic generation in aluminum nitride microrings with 2500%/W conversion efficiency, Optica **3**, 1126 (2016).

[29] S. Clemmen, K. P. Huy, W. Bogaerts, R. G. Baets, P. Emplit, and S. Massar, Continuous wave photon pair generation in silicon-on-insulator waveguides and ring resonators, Opt. Express **17**, 16558 (2009).

[30] J. W. Silverstone, D. Bonneau, K. Ohira, N. Suzuki, H. Yoshida, N. Iizuka, M. Ezaki, C. M. Natarajan, M. G. Tanner, R. H. Hadfield, V. Zwiller, G. D. Marshall, J. G. Rarity, J. L. O'Brien, and M. G. Thompson, On-chip quantum interference between silicon photon-pair sources, Nat. Photonics **8**, 104 (2014).

[31] X. Guo, C.-l. Zou, C. Schuck, H. Jung, R. Cheng, and H. X. Tang, Parametric down-conversion photon-pair source on a nanophotonic chip, Light Sci. Appl. **6**, e16249 (2017).

[32] C.-L. Zou, X.-D. Chen, X. Xiong, F.-W. Sun, X.-B. Zou, Z.-F. Han, and G.-C. Guo, Photonic simulation of system-environment interaction: Non-Markovian processes and dynamical decoupling, Phys. Rev. A **88**, 063806 (2013).

[33] X.-s. Ma, X. Guo, C. Schuck, K. Y. Fong, L. Jiang, and H. X. Tang, On-chip interaction-free measurements via the quantum Zeno effect, Phys. Rev. A **90**, 042109 (2014).

[34] Y. H. Wen, O. Kuzucu, M. Fridman, A. L. Gaeta, L.-W. Luo, and M. Lipson, All-Optical Control of an Individual Resonance in a Silicon Microresonator, Phys. Rev. Lett. **108**, 223907 (2012).

[35] K. T. McCusker, Y.-P. Huang, A. S. Kowligy, and P. Kumar, Experimental Demonstration of Interaction-Free All-Optical Switching via the Quantum Zeno Effect, Phys. Rev. Lett. **110**, 240403 (2013).

[36] S. M. Hendrickson, C. N. Weiler, R. M. Camacho, P. T. Rakich, A. I. Young, M. J. Shaw, T. B. Pittman, J. D. Franson, and B. C. Jacobs, All-optical-switching demonstration using two-photon absorption and the Zeno effect, Phys. Rev. A **87**, 023808 (2013).

[37] Y.-Z. Sun, Y.-P. Huang, and P. Kumar, Photonic Nonlinearities via Quantum Zeno Blockade, Phys. Rev. Lett. **110**, 223901 (2013).

[38] J.-Y. Chen, Y. M. Sua, Z.-T. Zhao, M. Li, and Y.-P. Huang, Observation of quantum Zeno blockade on chip, Sci. Rep. **7**, 14831 (2017).

[39] H. Jung, R. Stoll, X. Guo, D. Fischer, and H. X. Tang, Green, red, and IR frequency comb line generation from single IR pump in AlN microring resonator, Optica **1**, 396 (2014).

[40] J. B. Surya, X. Guo, C.-L. Zou, and H. X. Tang, Efficient third-harmonic generation in composite aluminum nitride/silicon nitride microrings, Optica **5**, 103 (2018).

[41] T. Tritschler, O. D. Mücke, M. Wegener, U. Morgner, and F. X. Kärtner, Evidence for Third-Harmonic Generation in Disguise of Second-Harmonic Generation in Extreme Nonlinear Optics, Phys. Rev. Lett. **90**, 217404 (2003).

[42] See Supplemental Material at http://link.aps.org/supplemental/10.1103/PhysRevLett.120.203902 for detailed theoretical derivation and experimental parameters.

[43] T. Carmon, L. Yang, and K. Vahala, Dynamical thermal behavior and thermal self-stability of microcavities, Opt. Express **12**, 4742 (2004).

[44] D. Grassani, S. Azzini, M. Liscidini, M. Galli, M. J. Strain, M. Sorel, J. E. Sipe, and D. Bajoni, Micrometer-scale integrated silicon source of time-energy entangled photons, Optica **2**, 88 (2015).

[45] J. W. Silverstone, R. Santagati, D. Bonneau, M. J. Strain, M. Sorel, J. L. O'Brien, and M. G. Thompson, Qubit entanglement between ring-resonator photon-pair sources on a silicon chip, Nat. Commun. **6**, 7948 (2015).

[46] Z. Vernon, M. Liscidini, and J. E. Sipe, Quantum frequency conversion and strong coupling of photonic modes using four-wave mixing in integrated microresonators, Phys. Rev. A **94**, 023810 (2016).